Available online at www.sciencedirect.com

ScienceDirect

Advances in Space Research 60 (2017) 1585–1593

ADVANCES IN SPACE RESEARCH (a COSPAR publication)

www.elsevier.com/locate/asr

Ionospheric winter anomaly and annual anomaly observed from Formosat-3/COSMIC Radio Occultation observations during the ascending phase of solar cycle 24

V. Sai Gowtam, S. Tulasi Ram *

Indian Institute of Geomagnetism, Navi Mumbai 410218, India

Received 20 January 2017; received in revised form 7 March 2017; accepted 12 March 2017
Available online 19 March 2017

Abstract

Ionospheric winter and annual anomalies have been investigated during the ascending phase of solar cycle 24 using high-resolution global 3D – data of the FORMOSAT – 3/COSMIC (Formosa satellite – 3/Constellation Observing System for Meterology, Ionosphere and Climate) radio occultation observations. Our detailed analysis shows that the occurrence of winter anomaly at low-latitudes is confined only to the early morning to afternoon hours, whereas, the winter anomaly at mid-latitudes is almost absent at all local times during the ascending phase of solar cycle 24. Further, in the topside ionosphere (altitudes of 400 km and above), the winter anomaly is completely absent at all local times. In contrast, the ionospheric annual anomaly is consistently observed at all local times and altitudes during this ascending phase of solar cycle 24. The annual anomaly exhibits strong enhancements over southern EIA crest latitudes during day time and around Weddle Sea Anomaly (WSA) region during night times. The global mean annual asymmetry index is also computed to understand the altitudinal variation. The global mean AI maximizes around 300–500 km altitudes during the low solar active periods (2008–10), whereas it extends up to 600 km during moderate to high (2011) solar activity period. These findings from our study provide new insights to the current understanding of the annual anomaly.

Keywords: Winter anomaly; Annual anomaly and radio occultation

1. Introduction

Anomalies in the F2 layer always puzzle the ionospheric research community. The solar zenith angle dependent Chapman's theory cannot explain the behavior of ionospheric F2 layer due to its complex dynamics and electrodynamic processes involved. Major anomalies of the ionosphere, equatorial ionization anomaly, winter/seasonal anomaly and semi-annual anomaly are relatively well studied and understood than the annual anomaly or non-seasonal anomaly. The physical mechanisms behind the ionospheric annual anomaly are still challenging and listed as one of the top scientific targets of the ionospheric community by Rishbeth (2007). Many studies in the past have described the winter and annual anomalies in the ionospheric F2-region. The winter or seasonal anomaly is defined as the greater F2-layer peak density (NmF2) values in the winter hemisphere than in the summer hemisphere during the solstices. The winter anomaly was first discovered by Berkner et al. (1936); and later Berkner and wells (1938) found that there was an annual anomaly too. From the global NmF2 maps, Torr and Torr (1973) concluded that the winter anomaly is maximum/minimum during the solar maximum/minimum. Recently, Burns et al. (2014) found that the winter anomaly is not seen during

* Corresponding author.
E-mail address: tulasi@iigs.iigm.res.in (S. Tulasi Ram).

http://dx.doi.org/10.1016/j.asr.2017.03.017
0273-1177/

low solar activity periods when the F10.7 solar flux is less than the threshold level of 90–100 solar flux units ($1 \text{ sfu} = 10^{-22} \text{ Wm}^{-2} \text{ Hz}^{-1}$). Further, Burns et al. (2014, 2015) concluded that the observed winter anomaly is due to greater winter to summer changes in the atomic oxygen to molecular nitrogen (O/N2) density ratio in solar maximum than in solar minimum.

In contrast, the ionospheric annual anomaly or non-seasonal anomaly is defined as, the world as a whole, December NmF2 values are significantly higher than those in June solstice. By analyzing paired ionosonde NmF2 data, Yonezawa and Arima (1959) found that the December NmF2 values are significantly higher than June. Later, Yonezawa (1971) concluded that the annual anomaly of NmF2 decreases with increasing latitude and solar activity during daytime as well as nighttime. Buonsanto (1986) suggested that the greater flux in December solstice causes greater dissociation of O_2 than June solstice may influence the production and loss coefficient of F2 layer. By analyzing topside ionospheric data, Su et al. (1998) discussed the role of neutral winds and ExB drift velocity in the annual anomaly. Further, they concluded that the ExB drift may significantly reduce the annual anomaly during daytime and enhance the anomaly during the post-sunset hours. Mendillo et al. (2005) used VTEC data to analyze the annual anomaly and found that the observed anomaly greatly exceeds the annual asymmetry of neutral atomic oxygen/molecular nitrogen ratio derived from the TIMED satellite data. From their model simulations using Coupled Thermosphere-Ionosphere-Plasmasphere (CTIP) model, Rishbeth and Muller-Wodarg (2006) attributed the observed annual anomaly could be due to the tidal forcing from the lower atmosphere. Zeng et al. (2008) studied the annual asymmetry by using Constellation Observing System for Meteorology, Ionosphere and Climate (COSMIC) radio occultation (RO) data during 2006 and they found that the annual asymmetry index shows two distinct maxima around local noon and midnight. Further, they found a significant longitudinal variation of the annual asymmetry around noon. From the case controlled simulations using TIEGCM (Thermosphere-Ionosphere-Electrodynamics Global Circulation Model), Zeng et al. (2008) have identified that varying Sun-Earth distance, offset between geographic and geomagnetic equator and the tilt of geomagnetic dipole axis are the main factors responsible for ionospheric annual anomaly and its longitudinal variability. Zeng et al. (2008) further shown that the tidal forcing from lower atmosphere has only a minor effect on annual anomaly.

Since both the winter and annual anomalies (seasonal and non-seasonal anomalies) are co-exist at the same time, it is often difficult to separate the effects of winter anomaly and annual anomaly. Rishbeth and Muller-Wodarg (2006) have raised a question whether the annual anomaly is simply due to stronger winter anomaly during the northern winter or it has a distinct physical cause. Burns et al. (2014) also expressed that weather the winter anomaly is independent of changes in annual anomaly or not. Further, most of the previous studies on annual anomaly are based on the NmF2 data from the paired ionosonde stations or total electron content (TEC) data, except a few (e.g., Zeng et al., 2008; Lee et al., 2011 and Burns et al., 2012), which limits the studies only to the lateral variations of annual anomaly. To the best of our knowledge, altitudinal variation of the annual anomaly is less studied in the past. Hence, in view of the above factors, the objective of the current paper is focused on the ionospheric annual anomaly and its local time, latitude, altitude and solar cycle variation in comparison with winter anomaly during the ascending phase of solar cycle 24.

2. Data

With a constellation of six microsatellites, the Constellation Observing System for Meteorology, Ionosphere and Climate (COSMIC/FORMOSAT-3) is primarily dedicated Radio Occultation (RO) mission to study the Earth's atmosphere and ionosphere. In this present study, we considered the vertical electron density profile data from COSMIC Radio Occultation experiment during ascending phase of solar cycle 24 (2008–2012) provided by University Corporation for Atmospheric Research COSMIC data Analysis and Archive center (UCAR – CDAAC) (http://www.cosmic.ucar.edu). The data corresponding to 41 days centered on June 21 ($\pm$20 days) and December 21 ($\pm$20 days) are used to represent June and December solstice respectively. Two step data quality control is applied to the raw data set. 1. Questionable electron density profiles with standard deviation greater than 1.5 are removed as suggested by Yang et al. (2009). 2. Disturbed days (with $Kp > 3$) are removed to analyze the quiet time variations, however, geomagnetically disturbed conditions are relatively rare and the contribution of such rare events to the 41 day mean is small (Burns et al., 2014). The 41-day mean solar flux values during the period of study are tabulated in Table 1.

3. Results

With a view to examine the local time and latitudinal behavior of the peak electron density of F2 layer, the NmF2 data from the COSMIC electron density profiles are binned in 30 min local time and 2.5° magnetic dip

Table 1
The 41-day mean F10.7 solar flux values centered on June 21 and December 21 along with the Global Mean AI during the years 2008–2012.

Year	F10.7 (solar flux units)			Global mean AI	
	June	December	ΔF10.7	Noon	Mid-night
2008	67.9610	67.0250	−0.9405	0.1468	0.1790
2009	70.9415	74.5732	3.6317	0.1997	0.2255
2010	75.5951	82.2400	6.6449	0.2438	0.2518
2011	96.3268	135.8250	39.4982	0.3368	0.4485
2012	134.8829	111.9859	−22.897	0.1008	0.1029

latitude grids. The NmF2 values in each grid which corresponds to various longitudinal regions are averaged to compute zonal mean NmF2 and a 5-point running mean is applied in both latitude and local time directions. Fig. 1 shows the local time and magnetic latitudinal variation of the zonally averaged NmF2 during June (a-e) and December (f-j) from 2008 to 2012. The respective summer and winter hemispheres during June and December solstices are indicated in the figure. From the Fig. 1, one can observe the local time variations of equatorial ionization anomaly and its interhemispheric asymmetry during solstices. During both the solstices, the NmF2 values in their respective winter hemispheres are higher than in the summer hemispheres during the morning to noon (0700–1200 LT) hours, particularly, at EIA crest and low-mid latitudes. This indicates the presence of winter anomaly at morning to noon during the ascending phase of solar cycle 24 (2008–2012) at low latitudes. However, by around noon to early afternoon hours (~1200–1300 LT), the winter anomaly subsides and the EIA crests in summer hemisphere become stronger than the winter EIA crests. Further, the larger NmF2 values in summer hemisphere are maintained throughout from afternoon to pre-dawn hours. Further, the subsidence of winter anomaly and the transition of stronger EIA crest from winter hemisphere to summer hemisphere occur slightly earlier in the December solstice (~1100–1200 LT) (right panels) than in June (~1300–1400 LT) (left panels). At middle and high latitudes, the NmF2 values in winter hemisphere are always smaller than in the summer hemisphere indicating that the winter anomaly is almost absent at mid-high latitudes during 2008–2012.

Another interesting feature that can be observed from Fig. 1 is that the NmF2 values are in general significantly higher during December solstice (right panels) than in June solstices (left panels) indicating the presence of annual anomaly consistently through 2008–2012. In order to separate the annual asymmetry from winter anomaly and to quantify the strength of annual asymmetry, Rishbeth and Muller-Wodarg (2006) suggested computing the annual asymmetry index (AI) by averaging the conjugate hemispheric NmF2 values, as

$$\mathrm{AI} = \frac{NmF2_{NS}(DEC) - NmF2_{NS}(Jun)}{NmF2_{NS}(DEC) + NmF2_{NS}(Jun)} \quad (1)$$

where

$$NmF2_{NS}(\theta,\lambda) = \frac{1}{2}\cdot[NmF2(\theta_N,\lambda) + NmF2(\theta_S,\lambda)] \quad (2)$$

Here, θ is geomagnetic latitude, λ is the geographic longitude; and N and S indicate the corresponding conjugate locations in northern and southern hemispheres, respec-

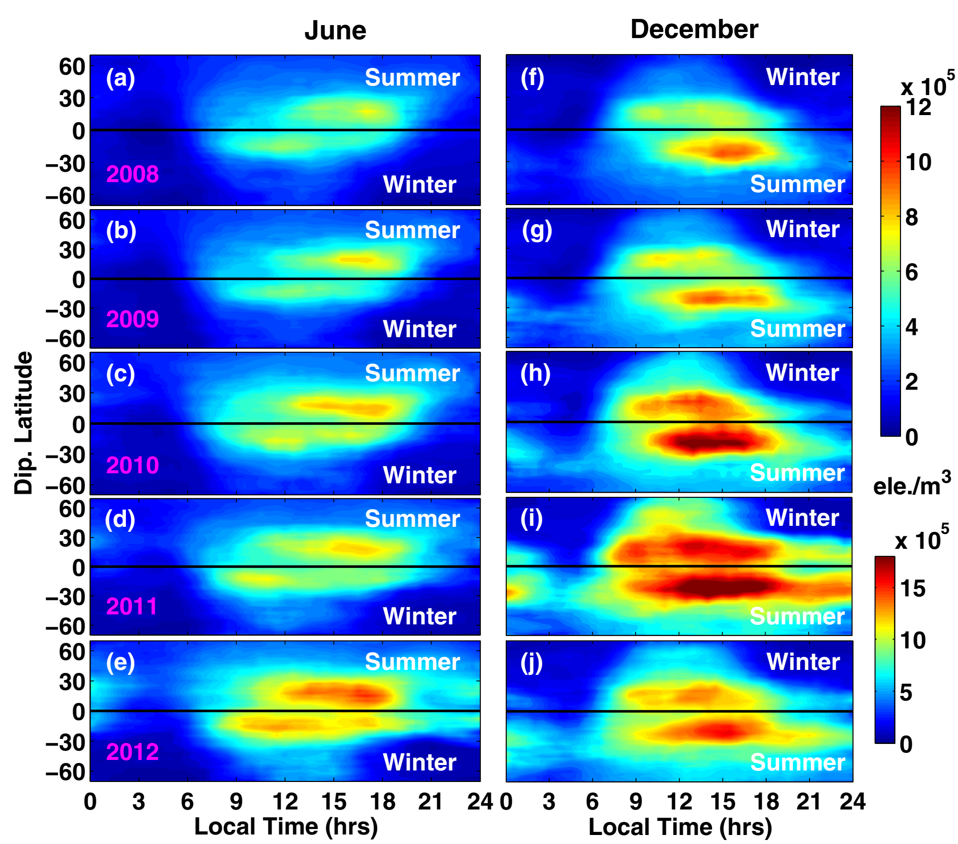

Fig. 1. Local time and latitudinal variation of the zonally averaged NmF2 during June (Left) and December (Right) solstice from 2008 to 2012. Solid black horizontal line represents the dip equator. (Note the different color scales used for 2008–2010 and 2011–2012 for better visibility). (For interpretation of the references to colour in this figure legend, the reader is referred to the web version of this article.)

tively. From Eq. (1), it can be understood that positive AI means that the NmF2 values in December solstices are greater than those in June solstice. For example, an AI of 0.2 (0.3) means that the NmF2 value in December is 50% (85%) higher than in June solstice.

Fig. 2 shows the local time and latitudinal variation of zonally averaged AI computed using (1) and (2) during 2008–2012. The solid black curve indicates the zero contour level. Nevertheless, the overall dominance of positive AI values indicate that the NmF2 values in December solstice are globally higher than in June solstice, confirms the existence of annual asymmetry throughout the ascending phase of solar cycle 24 at all local times. The AI values in 2011 are substantially larger, which could be due to increased F10.7 solar flux (solar activity) in December 2011 with respect to June 2011 (Table 1). Though the overall asymmetry is positive in 2012, the AI values are relatively smaller due to decrease in F10.7 solar flux during December 2012 compared to June 2012 (Table 1). Further, the local time variation of AI from Fig. 2 indicates that the annual anomaly is significantly enhanced around noon and mid-night periods with two broad maxima. This local time behavior with noon and mid-night enhancements is consistent with previous study by Zeng et al. (2008). The noontime enhancement in AI appears from latitudes greater than ∼15° and extends up to ∼50°–60° dip latitudes. The AI enhancement around mid-night hours starts from equatorial latitudes and extends up to mid-latitudes (40°–45° dip latitudes). Further, we computed the global mean AI around noon and mid-night periods during the ascending phase of solar cycle 24 which is tabulated in Table 1. One can see that the AI during mid-night is slightly higher than during the noon consistently through 2008–2012.

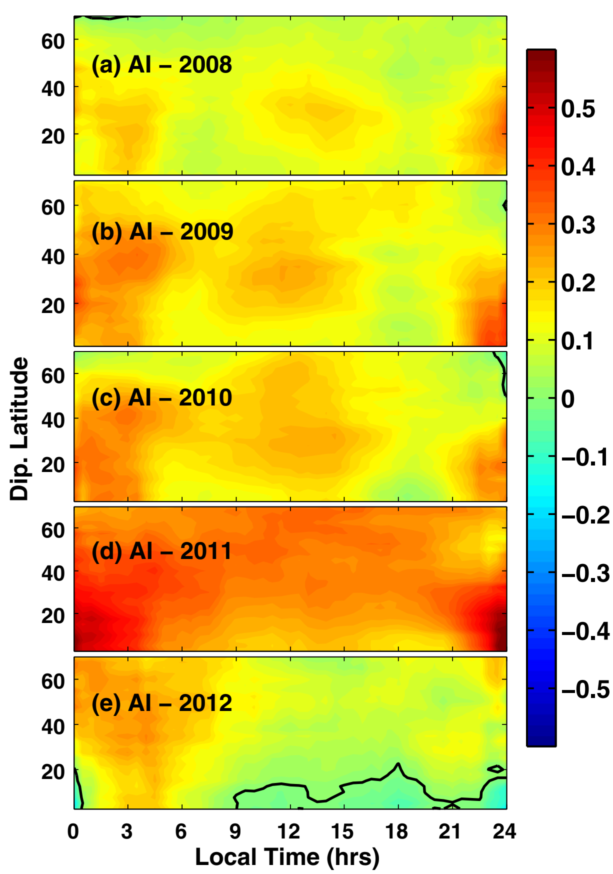

Fig. 2. Local time and latitudinal variation of zonally averaged AI from 2008 to 2012. Positive (negative) AI values indicate NmF2 values in December solstices are greater (smaller) than in June solstices. Solid black curve indicates the zero contour level.

Above mentioned results are based on the peak electron density of the F-layer. With a view to understand the altitudinal variation of ionospheric annual anomaly, the electron density values at fixed heights during 2009 are binned in 30 min local time and 2.5° magnetic dip latitude grids. To avoid the uneven solar flux values between June and December solstices and its influence on the annual anomaly, we selected June and December solstice of 2009 because of nearly comparable solar flux values (see Table 1). The electron density values in each grid which corresponds to various longitudinal regions are averaged to compute zonal mean electron density and a 5-point running mean is applied in both latitude and local time directions. It should be noted that the Abel inversion of RO observations often introduces a systematic error due to horizontal gradients in the ionosphere which violates the spherical symmetry assumption in Abel retrieval (Liu et al., 2010; Yue et al., 2010; Tulasi Ram et al., 2016). However, these errors in Abel inversion due to lateral inhomogenities are mostly below 200 km of equatorial and low latitudes (Liu et al., 2010; Yue et al., 2010). Hence, we excluded the COSMIC observations below 250 km in this analysis to safely avoid the errors due to spherical asymmetry in Abel retrieval.

Fig. 3 shows the local time and magnetic latitudinal variation of zonal mean electron density at different heights starting from 300 km to 700 km. The Left panels represent the June solstice and right panels represent the December solstice, respectively. From the Fig. 3, one can see that the equatorial ionization anomaly and its local time and altitudinal variation. During both the solstices, at 300 km altitude, the electron density values in their respective winter hemispheres are higher than the summer hemisphere during the morning to noon (0700–1200 LT) hours, particularly, at low and EIA crest latitudes. This indicates the existence of low latitude winter anomaly at morning to noon at an altitude of 300 km (Fig. 3(a) and (f)). However, by around noon to early afternoon hours (∼1200–1300 LT), the low latitude winter anomaly subsides and the EIA crests in summer hemisphere become stronger than the winter EIA crests. Further, the larger electron density values in summer hemisphere are maintained throughout from afternoon to pre-dawn hours. These observed local time and latitude variation of electron density at 300 km is similar to that of NmF2 data shown in Fig. 1. However, in the topside ionosphere where the double crest structure of EIA is mostly absent (at altitudes 400 km and above), the electron density values in their respective summer hemisphere are higher than the winter hemisphere during both

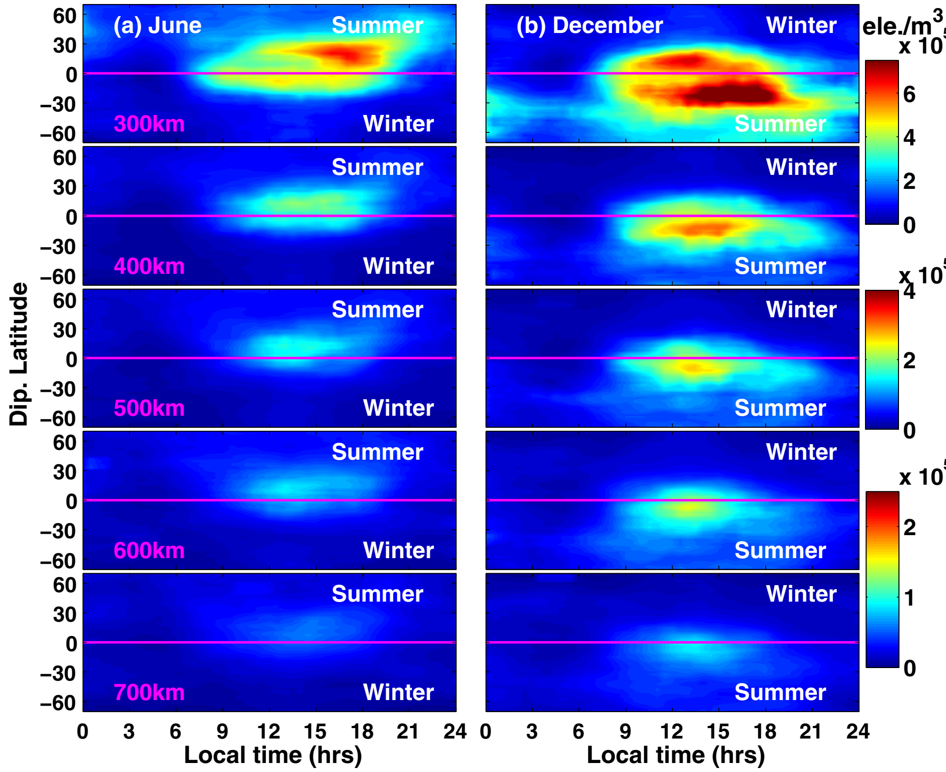

Fig. 3. Local time, latitudinal and altitudinal variation of the zonally averaged electron density during June (Left) and December (Right) solstice of the year 2009. Solid magenta horizontal line represents the dip equator. Each panel represents electron density variation at a given altitude as indicated in the panels.

the solstices and at all local times. Hence, we can conclude that the winter anomaly is confined only to lower latitudes and lower altitudes (below F2-peak) during this low solar activity period 2009. Another interesting observation from Fig. 3 is that the electron density values during December solstice (right panels) is significantly higher than those in June solstice (left panels) at all heights confirming that the annual anomaly exists at all heights. Further, the electron density values in the summer hemisphere of December solstice (southern summer) are significantly higher than in the summer hemisphere of June solstice (northern summer).

Results drawn from Figs. 1–3 are based on the zonally averaged NmF2 data. Any longitudinal and altitudinal variation in the annual anomaly cannot be resolved by this approach. Hence, in order to understand the longitudinal and altitudinal variation of the annual anomaly, electron density data around noon (1130–1230 LT) and midnight (2330–0030) hours during 2009 are binned in 5° longitude and 2.5° magnetic dip latitude grids at the altitudes starting from 300 km and above. The annual anomaly index (AI) is computed using Eqs. (1) and (2) by averaging electron density data at different altitudes starting from 300 km (±10 km) at every 100 km intervals (instead of NmF2). A 5-point running mean is applied in both longitude and magnetic latitude directions for smoothing. Fig. 4 shows the longitude, latitude and altitudinal variation of AI during noon (left panels) and midnight (right panels) periods of low solar activity year 2009. Solid black curve indicates zero contour level. Overall positive AI values around noon (Fig. 4a) indicate that the annual anomaly is distributed all over the globe. Further, the AI exhibits significant longitudinal variability. For example, at low to mid-latitudes (20°–45°), the AI exhibits broad enhancements around ∼170° W–90°W, ∼60°W–70°E and ∼120°E–180°E longitudes. The observed longitudinal variability consistently observed at all heights starting from 300 km and above. During midnight hours (Fig. 4b), one can see that a strong peak at mid-high latitudes at western (120°W–30°W) longitudes. This strong enhanced peak at high latitude is consistently observed at all heights. Further, enhancements in AI can be seen at low latitudes region over the longitudes from 60°W to 10°E and over the longitudes from 30°E to 10° E. From Fig. 4b, one can see that the observed low-latitude peaks around 60°W to 10°E longitudinal sectors are further decreases in magnitude with increase in altitude.

Further, the global mean AI is computed by averaging AI at all latitudes and longitudes at every 50 km interval starting from 250 km altitude to examine the altitudinal variation of global mean annual anomaly. Similar procedure is applied to the entire data set to understand the altitudinal variation of global mean AI during the ascending phase of solar cycle 24. Fig. 5 shows the altitudinal variation of the global mean AI computed around noon time (1130–1230 LT) during the ascending phase of the solar cycle 24. Overall positive values of global mean AI at any given altitude indicating that the annual anomaly exists at all heights during the entire ascending phase of solar

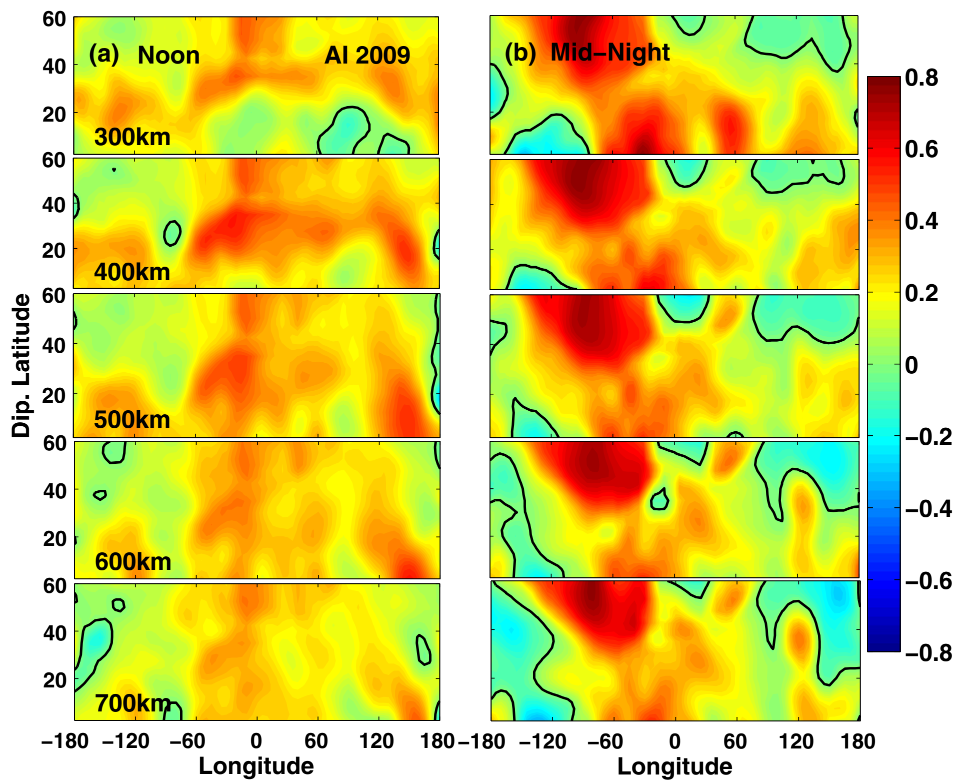

Fig. 4. Longitude, magnetic dip latitude and altitudinal variation of annual asymmetry index (AI) around noon (Left) and mid-night (Right) during 2009. Black solid curve represents zero contour level. Each panel represents AI variation at a given altitude as indicated in the panels.

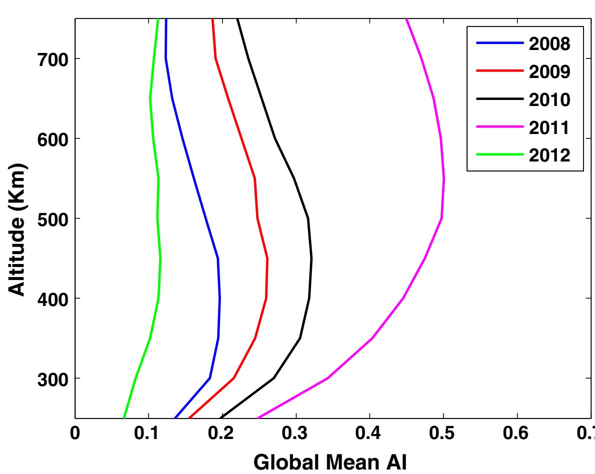

Fig. 5. Altitudinal variation of global mean AI during the ascending phase of solar cycle 24.

cycle 24. Further, AI maximizes around the altitude range of 300–500 km and then decreases gradually at higher altitudes during the years 2008–2010. Whereas the global mean AI values in 2011 are substantially larger at all heights, which could be due to significant increase of F10.7 solar flux value (solar activity) in December 2011 with respect to June 2011 (see Table 1). Though the overall AI at all heights is positive in 2012, the global mean AI values at all heights are relatively smaller due to decrease in F10.7 solar flux during December 2012 compared to June 2012.

4. Discussion

The winter anomaly, characterized by higher electron densities in the winter hemisphere than in the summer hemisphere during the solstices, can occur mainly due to two processes. At low latitudes, during solstices, the summer to winter hemispheric transequatorial neutral winds can transport the plasma from summer hemisphere to winter hemisphere causing higher plasma densities and intensified EIA crests in the winter hemisphere (Sastri, 1990; Walker, 1981; Rishbeth et al., 2000). The stronger EIA crests in the winter hemisphere observed from morning to local noon hours in Fig. 1 can be attributed to summer to winter hemispheric transequatorial neutral wind. Also, these stronger winter EIA crests during morning to noon hours were observed only at 300 km and F2 peak altitudes and not observed in the topside ionosphere (400 km and above). However, the equatorial zonal electric field and the associated equatorial fountain process maximizes by around noon hours (Raghavarao et al., 1978; Scherliess and Fejer, 1999). In winter hemisphere, the electrodynamic transport of plasma due to equatorial fountain process will be in the same direction to the transport due to transequatorial neutral wind. Therefore, the combined action of equatorial fountain and transequatorial wind push the plasma downward along the field lines into the region of higher recombination rate in the winter hemisphere causing weakening of winter EIA crests. On the other hand, the transport due to equatorial fountain process is in opposite direction to field aligned upward transport due to neutral wind in the summer hemisphere. As a result, the plasma accumulates at relatively higher altitudes (region of low recombination) and stronger EIA crests forms in the summer hemisphere. Balan and Bailey (1995) have shown that it is the effect of the neutral wind on the F-layer height that determines the hemisphere of the stronger EIA through model simulations. This interplay between transequatorial neutral wind and equatorial fountain processes explains the stronger EIA crests in the summer hemisphere during noon and afternoon hours observed in Fig. 1. Further, these results indicate that this distinct hemispheric behavior of EIA asymmetry, previously observed by Lin et al. (2007); Tulasi Ram et al. (2009) and Balan et al. (2013) during deep solar minimum period of 2007–2008, is consistently observed throughout the ascending phase of solar cycle 24. Further in the topside ionosphere (400 km and above) where the double peaked EIA structure is absent, the ionization in summer low latitudes is higher at all local times. The winter anomaly at middle and high latitudes is generally attributed to higher O/N2 density ratio in winter hemisphere than in summer hemisphere during the solstices (Rishbeth and Setty, 1961; Johnson, 1964). Further, Burns et al. (2014) have shown that the mid latitude winter anomaly stronger during high solar activity and does not occur during low solar activity periods when the F10.7 solar flux values becomes less than 90–100 sfu. From the present study (Figs. 1 and 3), it is further confirmed that the mid latitude winter anomaly not occurred during this ascending phase of solar cycle 24, even though, the F10.7 solar flux exceeded 100 sfu during 2011 and 2012.

In order to minimize the effects of winter anomaly on the annual anomaly Rishbeth and Muller-Wodarg (2006) suggested computing AI by averaging the conjugate hemispheric NmF2 values during June and December solstices as described in Eqs. (1) and (2). The computed AI variations shown in Figs. 2 and 4 indicate that the annual anomaly exists at all local times and altitudes consistently through this ascending phase of solar cycle 24. However, while averaging the conjugate hemispheric NmF2, one cannot examine the different levels (magnitudes) of annual anomaly in northern and southern hemispheres. Hence, we need a different approach to understand the differences in the hemispheric contributions to the annual anomaly at any given altitude. Further, from the results presented above, we can conclude that the winter anomaly is almost absent during the period of investigation except from morning to noon hours at low-latitudes. Hence, we can directly compute the solstice difference of electron density between December and June solstices ($\Delta Ne = Ne_{DEC}$ - $- Ne_{JUN}$) in order to understand the individual hemispheric contribution. For that, the electron density data around noon (1130–1230 LT) and mid-night (2300–0030 LT) hours during 2009 is binned in to 5° longitude and 2.5° latitude grids at the altitudes starting from 300 km and above. We selected the year 2009 because the F10.7 solar flux values are nearly comparable during June and December solstices in this year. Then the solstice difference in electron density (henceforth, ΔNe) is computed by subtracting the electron density values during June solstice from the December solstice. A 5-point running mean is applied in both longitude and latitude directions to get smooth variations. Fig. 6 shows the longitudinal and latitudinal variation of the solstice difference of electron density (ΔNe). Left panel represents noon (6a-e) and the right panel represents mid-night (6f-j). Solid black line represents the zero contour level. Positive ΔNe means electron density values during December solstice is higher than June solstice indicating the presence of annual anomaly. From the Fig. 6, one can observe the hemispheric differences in the annual anomaly. During noon at 300 km altitude (Fig. 6a), ΔNe is positive in the southern hemisphere and low latitudes of northern hemisphere. On the other hand, ΔNe is negative from middle to high latitudes of northern hemisphere indicating the absence of annual anomaly in the northern mid-high latitudes. At altitudes of 400 km and above (Fig. 6b–e), positive electron density values are confined mainly to the southern hemisphere. Two important results can be drawn from these observations. First, in the absence of winter anomaly during this low and ascending phase of solar cycle 24, the plasma density in the respective summer hemisphere is larger than in the winter hemisphere during both the solstices. That means, in the northern hemisphere, ΔNe ($Ne_{DEC} - Ne_{JUN}$) which represents the winter minus summer becomes negative. Whereas ΔNe in the southern hemisphere that represents the summer minus winter becomes positive. Second, the magnitudes of the positive ΔNe values in southern hemisphere are significantly higher than the negative ΔNe values in the northern hemisphere. This indicates that the electron density values in the southern summer (during December) are significantly higher than in northern summer (June) indicating that the major contribution to the ionospheric annual anomaly comes from the "southern summer" hemisphere which is consistently observed at all altitudes (see Fig. 6).

The significantly strong and positive ΔNe values at southern EIA crest latitudes during noon (Fig. 6a) can be attributed to formation of stronger summer EIA crests at relatively higher altitudes in the summer hemisphere due to the interplay of equatorial fountain process and transequatorial neutral as discussed above. During the midnight (Fig. 6b), the ΔNe exhibits strong positive values at middle and high latitudes of 120°W–30°W longitudes. These enhancements in ΔNe at western high latitudes are mainly due to the presence of Weddell Sea anomaly (WSA) during the December solstices (He et al., 2009; Jee et al., 2009; Lin et al., 2009, 2010; Chen et al., 2011). This enhancement of ΔNe over Weddell Sea Anomaly (WSA) region is consistently observed at all heights from 300 to 700 km and is responsible for enhanced AI values during midnight shown in Fig. 4b. The WSA is mainly attributed to equatorward neutral winds in the presence of southward offset of geomagnetic equator over the WSA region. Therefore, it is

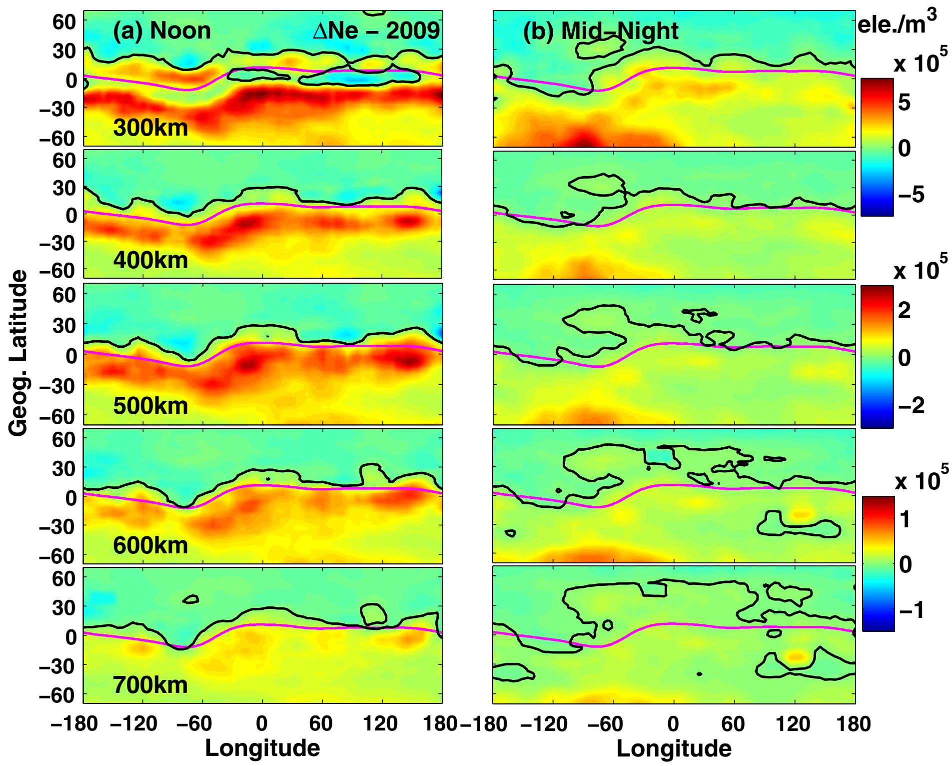

Fig. 6. Longitude, latitude and altitudinal variation of ΔNe during noon (Left) and midnight (Right) hours of 2009. Black solid curve represents zero contour level. Each panel represents ΔNe variation at a given altitude as indicated in the panels.

stressed that the neutral winds play significant role on the ionospheric annual anomaly during both day and night times. The detailed mechanisms and responsible factors for the ionospheric annual anomaly during both day and night times are further necessary. The role of neutral winds in the presence of geomagnetic field configuration on the local time and longitudinal variability of annual anomaly will be the focus of our future study through model simulations.

5. Conclusions

A detailed study on ionospheric winter anomaly and annual anomaly and the differences in their local time, latitude, longitude, altitude and solar cycle variability has been carried out using Formosat-3/COSMIC Radio Occultation observations during the ascending phase of solar cycle 24. The important findings from this study are briefly summarized hereunder. The occurrence of winter anomaly at low-latitudes is confined only to morning to noon hours at 300 km and F2-peak altitudes. The winter anomaly at mid-latitudes is almost absent at all local times during this ascending phase of solar cycle 24. Further, in the topside ionosphere (altitudes of 400 km and above), the electron density values in the respective summer hemisphere are higher than the winter hemisphere at all local times indicating the complete absence of winter anomaly. On the other hand, the ionospheric annual anomaly exists at all local times and altitudes consistently during this ascending phase of solar cycle 24. The local time variability of annual anomaly index (AI) exhibits broad enhancements around noon and midnight hours. The annual anomaly exhibits strong enhancements at southern EIA crest latitudes during noon due to the interplay between equatorial fountain process and transequatorial neutral wind; and around Weddle Sea Anomaly (WSA) region during night times. The global mean AI maximizes around 300–500 km altitude during low solar activity years 2008–2010 and decreases gradually at higher altitudes. These results provide better insights on the ionospheric winter and annual anomalies and their spatial and temporal variabilities.

Acknowledgements

The work of S. Tulasi Ram is supported by Department of Science and Technology (DST), Govt. of India through India-Taiwan Science and Technology cooperation project (GITA/DST/TWN/P-47/2013). We acknowledge the UCAR-CDAAC (http://cosmic-io.cosmic.ucar.edu/cdaac/index.html) for the Formosat-3/COSMIC RO data.

References

Balan, N., Rajesh, P.K., Sripathi, S., Tulasiram, S., Liu, J.Y., Bailey, G.J., 2013. Modeling and observations of the north-south ionospheric asymmetry at low latitudes at long deep solar minimum. Adv. Space Res. 52, 375–382. http://dx.doi.org/10.1016/j.asr.2013.04.003.

Balan, N., Bailey, G.J., 1995, Equatorial plasma fountain and its effects: possibility of an additional layer. J. Geophys. Res. 100(A11), 21,421–21,432. doi:http://dx.doi.org/10.1029/95JA01555.

Berkner, L.V., Wells, H.W., 1938. Non-seasonal change of F2-region ion density. Terr. Magn. Atmos. Electr. 43, 15–36.

Berkner, L.V., Wells, H.W., Seaton, S.L., 1936. Characteristics of the upper region of the ionosphere. Terr. Magn. Atmos. Electr. 41, 173–184.

Buonsanto, M.J., 1986. Possible effects of the changing Earth-Sun distance on the upper atmosphere. S. Pacific J. Nat. Sci. 8, 58–65.

Burns, A.G., Solomon, S.C., Wang, W., Qian, L., Zhang, Y., Paxton, L.J., 2012. Daytime climatology of ionospheric NmF2 and hmF2 from COSMIC data. J. Geophys. Res. 117, A09315. http://dx.doi.org/10.1029/2012JA017529.

Burns, A.G., Wang, W., Qian, L., Solomon, S.C., Zhang, Y., Paxton, L.J., Yue, X., 2014. On the solar cycle variation of the winter anomaly. J. Geophys. Res. Space Phys. 119, 4938–4949. http://dx.doi.org/10.1002/2013JA019552.

Burns, A.G., Solomon, S.C., Wang, W., Qian, L., Zhang, Y., Paxton, L.J., Yue, X., Thayer, J.P., Liu, H.L., 2015. Explaining solar cycle effects on composition as it relates to the winter anomaly. J. Geophys. Res. Space Phys. 120, 5890–5898. http://dx.doi.org/10.1002/2015JA021220.

Chen, C.H., Huba, J.D., Saito, A., Lin, C.H., Liu, J.Y., 2011. Theoretical study of the ionospheric Weddell Sea Anomaly using SAMI2. J. Geophys. Res. 116, A04305. http://dx.doi.org/10.1029/2010JA015573.

He, M., Liu, L., Wan, W., Ning, B., Zhao, B., Wen, J., Yue, X., Le, H., 2009. A study of the Weddell Sea Anomaly observed by FORMOSAT-3/COSMIC. J. Geophys. Res. 114, A12309. http://dx.doi.org/10.1029/2009JA014175.

Jee, G., Burns, A.G., Kim, Y.-H., Wang, W., 2009. Seasonal and solar activity variations of the Weddell Sea Anomaly observed in the TOPEX total electron content measurements. J. Geophys. Res. 114, A04307. http://dx.doi.org/10.1029/2008JA013801.

Johnson, F.S., 1964. Composition changes in the upper atmosphere. In: Thrane, E. (Ed.), Electron Density Distributions in the Ionosphere and Exosphere. North Holland, Amsterdam, pp. 81–84.

Lee, W.K., Kil, H., Kwak, Y.-S., Wu, Q., Cho, S., Park, J.U., 2011. The winter anomaly in the middle-latitude F region during the solar minimum period observed by the Constellation Observing System for Meteorology, Ionosphere and Climate. J. Geophys. Res. 116, A02302. http://dx.doi.org/10.1029/2010JA015815.

Lin, C.H., Liu, C.H., Liu, J.Y., Chen, C.H., Burns, A.G., Wang, W., 2010. Midlatitude summer nighttime anomaly of the ionospheric electron density observed by FORMOSAT-3/COSMIC. J. Geophys. Res. 115, A03308. http://dx.doi.org/10.1029/2009JA014084.

Lin, C.H., Liu, J.Y., Cheng, C.Z., Chen, C.H., Liu, C.H., Wang, W., Burns, A.G., Lei, J., 2009. Three dimensional ionospheric electron density structure of the Weddell Sea Anomaly. J. Geophys. Res. 114, A02312. http://dx.doi.org/10.1029/2008JA013455.

Lin, C.H., Liu, J.Y., Fang, T.W., Chang, P.Y., Tsai, H.F., Chen, C.H., Hsiao, C.C., 2007. Motions of the equatorial ionization anomaly crests imaged by FORMOSAT-3/COSMIC. Geophys. Res. Lett. 34, L19101. http://dx.doi.org/10.1029/2007GL030741.

Liu, H., Thampi, S.V., Yamamoto, M., 2010. Phase reversal of the diurnal cycle in the midlatitude ionosphere. J. Geophys. Res. 115, A01305. http://dx.doi.org/10.1029/2009JA014689.

Mendillo, M., Huang, C.-L., Pi, X., Rishbeth, H., Meier, R., 2005. The global ionospheric asymmetry in total electron content. J. Atmos. Sol. Terr. Phys. 67, 1377–1387.

Raghavarao, R., Sharma, P., Sivaraman, M.R., 1978. Correlation of ionization anomaly with the intensity of electrojet. Space Res. 18, 277–280.

Rishbeth, H., 2000, The equatorial F-layer: progress and puzzles, Ann. Geophys. 18, 730–739. doi:http://dx.doi.org/10.1007/s00585-000-0730-6.

Rishbeth, H., 2007. Thermospheric targets. Eos. Trans. AGU 88 (17), 189.

Rishbeth, H., Setty, C.S.G.K., 1961. The F-layer at sunrise. J. Atmos. Solar-Terr. Phys. 21, 263–276.

Rishbeth, H., Muller-Wodarg, I.C.F., 2006. Why is there more ionosphere in January than in July? The annual asymmetry in the F2-layer. Ann. Geophys. 24, 3293–3311.

Sastri, J.H., 1990. Equatorial anomaly in F region: a review. Indian J. Radio Space Phys. 19, 225–240.

Scherliess, L., Fejer, B.G., 1999. Radar and satellite global equatorial F region vertical drift model. J. Geophys. Res. 104 (A4), 6829–6842.

Su, Y.Z., Bailey, G.J., Oyama, K.I., 1998. Annual and seasonal variations in the low-latitude topside ionosphere. Ann. Geophys. 16, 974–985.

Torr, M.R., Torr, D.G., 1973. The seasonal behavior of the F2-layer of the ionosphere. J. Atmos. Solar-Terr. Phys. 35 (12), 2237–2251.

Tulasi Ram, S., Su, S.-Y., Liu, C.H., 2009. FORMOSAT-3/COSMIC observations of seasonal and longitudinal variations of equatorial ionization anomaly and its interhemispheric asymmetry during the solar minimum period. J. Geophys. Res. 114, A06311. http://dx.doi.org/10.1029/2008JA013880.

Tulasi Ram, S., Su, S.Y., Tsai, L.C., Liu, C.H., 2016. A self-contained GIM-aided Abel retrieval method to improve GNSS-Radio Occultation retrieved electron density profiles. GPS Solut. 20, 825–836. http://dx.doi.org/10.1007/s10291-015-0491-z.

Walker, G.O., 1981. Longitudinal structure of the equatorial ionization anomaly: a review. J. Atmos. Terr. Phys. 43, 763–775. http://dx.doi.org/10.1016/ 0021-9169(81)90052-0.

Yang, K.F., Chu, Y.H., Su, C.L., Ko, H.T., Wang, C.Y., 2009. An examination of FORMOSAT- 3/COSMIC ionospheric electron density profile: data quality criteria and comparisons with the IRI model. Terr. Atmos. Ocean. Sci. 20, 193–206. http://dx.doi.org/10.3319/TAO.2007.10.05.01 (F3C).

Yonezawa, T., 1971. The solar-activity and latitudinal characteristics of the seasonal, non-seasonal and semi-annual variations in the peak electron densities of the F2-layer at noon and at midnight in middle and low latitudes. J. Atmos. Sol. Terr. Phys. 33, 887–907.

Yonezawa, T., Arima, Y., 1959. On the seasonal and non-seasonal annual variations and the semi-annual variation in the noon and midnight electron densities of the F2 layer in middle latitudes. J. Radio Res. Labs. 6, 293–309.

Yue, X., Schreiner, W.S., Lei, J., Sokolovskiy, S.V., Rocken, C., Hunt, D. C., Kuo, Y.-H., 2010. Error analysis of Abel retrieved electron density profiles from radio occultation measurements. Ann. Geophys. 28, 217–222. http://dx.doi.org/10.5194/angeo-28-217-2010.

Zeng, Z., Burns, A., Wang, W., Lei, J., Solomon, S., Syndergaard, S., Qian, L., Kuo, Y.-H., 2008. Ionospheric annual asymmetry observed by the COSMIC radio occultation measurements and simulated by the TIEGCM. J. Geophys. Res. 113, A07305. http://dx.doi.org/10.1029/2007JA012897.